Closing the Plio-Pleistocene ^{13}C cycle in the 405-kyr periodicity by isotopic signatures of geological sources

Peter Köhler[1]

[1]Alfred-Wegener-Institut Helmholtz-Zentrum für Polar- und Meeresforschung, P.O. Box 12 01 61, 27515 Bremerhaven, Germany

Correspondence: Peter Köhler (peter.koehler@awi.de)

Abstract.

The ^{13}C cycle of the Plio-Pleistocene, as recorded in δ^{13}C of benthic foraminifera, has power in periodicities related to the long eccentricity cycle of 405-kyr that is missing in corresponding climate records (e.g. δ^{18}O). Using a global carbon cycle model I show that the long eccentricity in δ^{13}C might have been caused by variations in the isotopic signature of geological

5 sources, namely of the weathered carbonate rock (δ^{13}C$_{\mathrm{rock}}$) or of volcanically released CO$_2$ (δ^{13}C$_{\mathrm{v}}$). This closure of the ^{13}C cycle in these peridicities also explains the offset in atmospheric δ^{13}CO$_2$ seen between the penultimate and the last glacial maximum. The necessary isotopic signatures in δ^{13}C$_{\mathrm{rock}}$ or δ^{13}C$_{\mathrm{v}}$ which align my simulations with reconstructions of the ^{13}C cycle on orbital timscales have most power in the obliquity band (41-kyr) suggesting that land ice dynamics are the ultimate cause for these suggested variations. Since the Asian monsoon as reconstructed from speleothems has also an obliquity-related

10 component it is possible that these proposed changes in weathering are indeed, at least partly, connected to the monsoon as previously suggested. Alternatively, the suggested impact of land ice or sea level on volcanic activity might also be influential for the ^{13}C cycle. This indirect influence of ice sheets on the long eccentricity cycle in δ^{13}C implies that these processes might not have been responsible for the 405-kyr periodicity found in ice-free times of the pre-Pliocene parts of the Cenozoic.

1 Introduction

15 The long eccentricity cycle with a periodicity of 405-kyr is for the last 5 Myr missing in most climate signals, e.g. in the benthic $\delta^{18}O$ (Lisiecki and Raymo, 2005), but is imprinted on the global carbon cycle since significant power in it is contained in benthic $\delta^{13}C$ (e.g. Mix et al., 1995b; Wang et al., 2010). For earlier parts of the Cenozoic the 405-kyr cycle is not only found in $\delta^{13}C$ but also in $\delta^{18}O$ (Pälike et al., 2006; Zeebe et al., 2017; De Vleeschouwer et al., 2020; Westerhold et al., 2020). This difference between climate and carbon cycle makes the interpretation of the Plio-Pleistocene $\delta^{13}C$ signature and related

20 interpretations with respect to processes responsible for changes in atmospheric CO_2 challenging.

Some interpretations of the impact of long eccentricity on $\delta^{13}C$ have been put forward. Russon et al. (2010) used a carbon cycle box model to analyse how oceanic processes, e.g. small changes in nutrient availability or in the ratio of organic matter to $CaCO_3$ in the export production, might have caused these $\delta^{13}C$ changes. They already point out that changes in only the ^{13}C cycle but not atmospheric CO_2, and therefore global climate, are difficult to explain. Ma et al. (2011) used a slightly different

25 box model and proposed that eccentricity impacts on the weathering intensity and nutrient supply ultimately changed $\delta^{13}C$ in $\sim$400-kyr periodicity during the Miocene. Paillard (2017) used a conceptual model and suggested that riverine organic carbon inputs into the ocean caused by sea level related erosion at river mouths might be responsible for $\sim$400-kyr variability in $\delta^{13}C$ of the last 4 Ma. In a data review Wang et al. (2014) also proposed that the origin of this low $\delta^{13}C$ frequency is related to riverine input, but suggested that the underlying process is the monsoon intensity.

30 While the long-term changes in $\delta^{13}C$ in the ocean have long been known (e.g. Mix et al., 1995b) the record of $\delta^{13}CO_2$ from ice cores is still relatively new and with 155 kyr rather short (Eggleston et al., 2016). Upcoming new ice core data across Termination IV (around 340 kyr BP) might in the near future offer another $\sim$10 kyr long snapshot of changes in $\delta^{13}CO_2$ (Krauss, 2024). When $\delta^{13}CO_2$ data across Termination II were first measured (Schneider et al., 2013) an apparent offset between the Penultimate and the Last Glacial Maximum (PGM and LGM, respectively) of +0.45‰ prevented a straight-

35 forward interpretation of the data. Among other possibilities the authors speculated that geological processes, namely changes in the isotopic ratio of carbonate weathering or in the contributions from volcanic input fluxes, might explain this offset in $\delta^{13}CO_2$. However, it was not yet discussed in the ice core community (Schneider et al., 2013; Eggleston et al., 2016) if the PGM-to-LGM offset in $\delta^{13}CO_2$ and the long eccentricity cycle in benthic $\delta^{13}C$ are related to each other.

Here, I use the well-established global carbon cycle box model BICYCLE-SE (Köhler and Munhoven, 2020) to test in

40 detail, if these geological processes proposed by Schneider et al. (2013) might indeed be responsible for PGM-to-LGM offset in $\delta^{13}CO_2$ and eventually also for the changes in the ^{13}C cycle related to the long eccentricity. For that effort I first reanalyse previously published simulations which have been performed with an updated ^{13}C cycle over the time window covered by $\delta^{13}CO_2$ (Köhler and Mulitza, 2024). In that study atmospheric $\delta^{13}CO_2$ was in some simulations already prescribed by the ice core data, and not internally calculated in the model. This approach indirectly introduced some long-term variability in $\delta^{13}C$

45 to the whole ^{13}C cycle, while the boundary conditions changing the main carbon cycle and CO_2 were not modified. I first analyse if and how these changes in ^{13}C necessary for $\delta^{13}CO_2$ to agree with ice cores reconstructions might have been caused by the two geological processes of interest. I then add further scenarios to my assessment, in which one variable of the ^{13}C

cycle in the model is not prescribed by data, but only weakly nudged to a δ^{13}C time series. This nudging approach reduces the amount of necessary adjustments considerably and is first applied to atmospheric $\delta^{13}CO_2$, and then expanded to deep ocean

50   δ^{13}C in order to be able to cover simulations longer than 155 kyr. Building on earlier work I then extend my investigation to simulations covering the ice core time window of the last 800 kyr (Köhler and Munhoven, 2020) and finally the last 5 Myr covering most of the Plio-Pleistocene (Köhler, 2023). As a side effect my nudging approach might also increase the simulated glacial-interglacial (G-IG) amplitudes in δ^{13}C in the earlier parts of the Plio-Pleistocene and bring them in better agreement with reconstructions (Köhler and Bintanja, 2008).

2 Methods

2.1 Data

I briefly summarise here the data to which I later compare my simulation results.

2.1.1 Plio-Pleistocene deep ocean time series

Due to the large volume of the Pacific ocean whole ocean changes in δ^{13}C are to a first order approximated with benthic δ^{13}C

60   data from the deep Pacific. Under this premise a deep Pacific δ^{13}C stack consisting of six sediment cores (Lisiecki, 2014) illustrates the variability in oceanic δ^{13}C over the last 3 Myr (Figure 1b), which is in its long-term variability, but with higher short-term scatter and a by 0.1‰ lower long-term mean, nicely matched by δ^{13}C from ODP846 (Mix et al., 1995a; Shackleton et al., 1995), which is also one of the cores contributing to the stack. This core ODP846 (3307 m water depth, 91°W close to the equator) extends further back in time and is used here as published in Poore et al. (2006) in order to cover a 5 Myr long

65   time window (Figure 1b).

     Stacking of cores always introduces a smoothing effect. Therefore, the width of the data distribution of the both time series converge to each other ($\sigma \approx 0.20$), if a 5-points-running mean is applied to the ODP846 data (Figure 1c), which in its raw data is more widely distributed ($\sigma = 0.26$). Both deep Pacific δ^{13}C time series contain significant power in periods longer than 100 kyr in their wavelets (Figure 1d,e), not only around 405-kyr ($\sim$500-kyr in the last 1 Myr), but also in-between the eccentricity

70   bands ($\sim$200-kyr periodicities). While the latter variability is not known from orbital forcing, it has already been detected before in terrestrial sediments of the early Paleocene, and might be a sub-harmonic of the 405-kyr periodicity (Hilgen et al., 2020). Alternatively, this power might be related to the 173-kyr periodicity, an amplitude modulation of the 41-kyr of obliquity, which is also found in the Miocene-Pliocene of Asian monsoon (Zhang et al., 2022) and in total organic carbon during the Mesozoic and Cenozoic (Huang et al., 2021). Power in periodicity in-between 100 and 405 kyr during the last 5 Myr are also

75   contained in previous wavelet analysis of so-called benthic δ^{13}C mega-splices, but they have never been discussed in more detail (De Vleeschouwer et al., 2020; Westerhold et al., 2020).

     Spectral analyses of various climate variables find little of these slow changes during the Plio-Pleistocene. The Prob-stack (Ahn et al., 2017), the successor to the LR04 benthic δ^{18}O stack (Lisiecki and Raymo, 2005) based on 180 instead of 57 records,
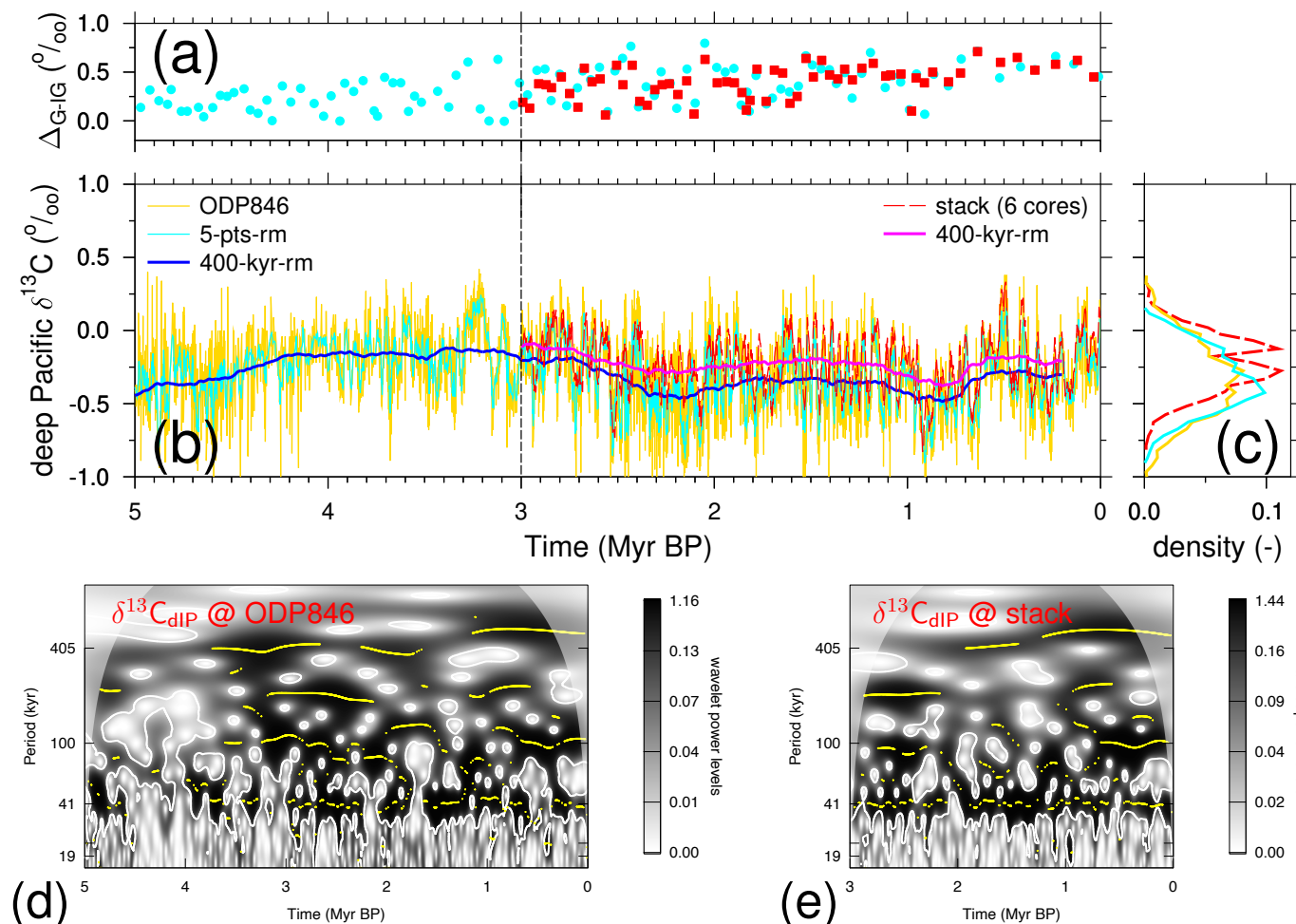
Figure 1. Deep Pacific Plio-Pleistocene δ^{13}C data based on either ODP846 (Mix et al., 1995a; Shackleton et al., 1995; Poore et al., 2006), or a stack from six cores (Lisiecki, 2014). The temporal resolution is 1 kyr in the stack and partly up to 2 kyr in ODP846, which are interpolated to equidistant 1 kyr for further analysis. **(a)** G-IG amplitudes of records showing in (b). Here the difference between a glacial minima and the subsequent interglacial maxima are calculated following the MIS boundary definition of Lisiecki and Raymo (2005) with points being positioned at mid-transitions. **(b)** Time series. 400-kyr running means are added as is a 5-points running mean of ODP846 to improve comparison to the stack. The vertical line at 3 Myr BP marks the start point of the records for the analysis shown in (c). **(c)** Normalised data density distribution of the last 3 Myr of the δ^{13}C time series shown in (b). **(d)** Wavelet of the 5-Myr long 5-points running mean of δ^{13}C from ODP846. **(e)** Wavelet of the 3-Myr long deep Pacific δ^{13}C stack.

contains little power in 405-kyr periodicity during the last 2.5 Myr, but some power earlier-on (Figure S1b,c), similarly as δ^{18}O

80 in ODP846, the deep Pacific core from which δ^{13}C is used here (Mix et al., 1995a; Shackleton et al., 1995; Poore et al., 2006) (Figure S1b,d). This long eccentricity cycle is also missing in the last 2.5-Myr and only weakly contained earlier in time series of my simulated atmospheric CO_2 (Figure S1e). For the interpretation of the rather unusual frequencies around 200-kyr in

δ^{13}C and the absence of the long eccentricity in δ^{18}O one should keep in mind that the response of a nonlinear system might exhibit frequencies not present in the original driven forcing (e.g. Rial, 1999; Rial et al., 2004).

85   Furthermore, during the Mid-Pleistocene Transition (MPT) around 1 Myr ago climate changed from a dominantly 41-kyr periodicity during the Pliocene and Early Pleistocene to an on average 100-kyr periodicity in the Late Pleistocene (e.g. Shackleton and Opdyke, 1976; Pisias and Moore-Jr., 1981). Since there is hardly any change in incoming solar radiation with power in the 100-kyr band (Laskar et al., 2004) this MPT is still not completely understood, but has so far been hypothesised to be caused by non-linear processes in the carbon cycle-climate system (e.g. Willeit et al., 2019; Berends et al., 2021; Clark

90 et al., 2024). An accompanying feature of the MPT is the rise in G-IG amplitudes, as for example seen in benthic δ^{18}O (Lisiecki and Raymo, 2005; Ahn et al., 2017) or in global temperature compilations (Clark et al., 2024). Benthic δ^{13}C also includes this transition in power from 41-kyr to 100-kyr frequency across the MPT (e.g. Köhler and Bintanja, 2008). However, G-IG amplitudes in benthic δ^{13}C only gradually increase over the Plio-Pleistocene. The size of these amplitudes is in both the deep Pacific core ODP846 or the deep Pacific stack in the 41-kyr world on average 68–76% of their mean amplitude found

95 in the 100-kyr world of the last 1 Myr (Figure 1a). This is markly different from benthic δ^{18}O whose G-IG amplitudes in the 41-kyr world have been on average only 35-39% of their size during the last 1 Myr (Figure S1a).

    These two aspects — long eccentricity cycle and G-IG amplitudes — in which δ^{13}C differs from climate variables during the Plio-Pleistocene suggests that the carbon cycle and the climate system are on orbital timescales partly decoupled.

2.1.2   Late Pleistocene surface ocean δ^{13}C and atmospheric δ^{13}CO$_2$

100 The continuous 155-kyr-long time series of atmospheric δ^{13}CO$_2$ (Eggleston et al., 2016) has been shown to be highly correlated, especially on orbital time scales, to two mono-specific stacks of δ^{13}C from planktic foraminifera in the wider tropics (Köhler and Mulitza, 2024). This latter study could not identify any impact of the so-called carbonate ion effect proposed from laboratory experiments (Spero et al., 1997), which is why the planktic δ^{13}C stacks can be considered as reliable recorders of δ^{13}C in dissolved inorganic carbon (δ^{13}C$_{\text{DIC}}$) in the surface ocean of the wider tropics. Underlying data were compiled from

105 sediments cores at latitudes <40°, roughly in agreement with the non-polar (sometimes called equatorial) surface ocean boxes in the model. To my knowledge there exists no robust longer time series of planktic δ^{13}C. Due to the shortness of these time series a spectral analysis with focus on the long eccentricity cycle is not possible. However, these data might help nevertheless via a comparison with simulation results.

2.1.3   The δ^{13}C signature of the geological source of carbonate weathering

110 Present day mountains have been built during the Phanerozoic (the last 540 Myr), but there exist also various areas with Precambrian shields (older than 540 Myr), e.g. in North America (e.g. Whitmeyer and Karlstrom, 2007; Faccenna et al., 2021). It is thus worth considering how δ^{13}C in carbonate rocks (δ^{13}C$_{\text{rock}}$) changed over these time spans. The records of δ^{13}C in carbonates during the Phanerozoic (Fig. 2b) varied for most of the last 440 Myr between 0 and +5‰ with short-term excursions up to +8‰ and –5‰ (Bachan et al., 2017). The earliest part of the Phanerozoic (440–540 Myr) covering the Cambrian and

115 Ordovician contained in generally lower values (–5 to 0‰) with peaks up to +7‰ (Bachan et al., 2017). A compilation of raw
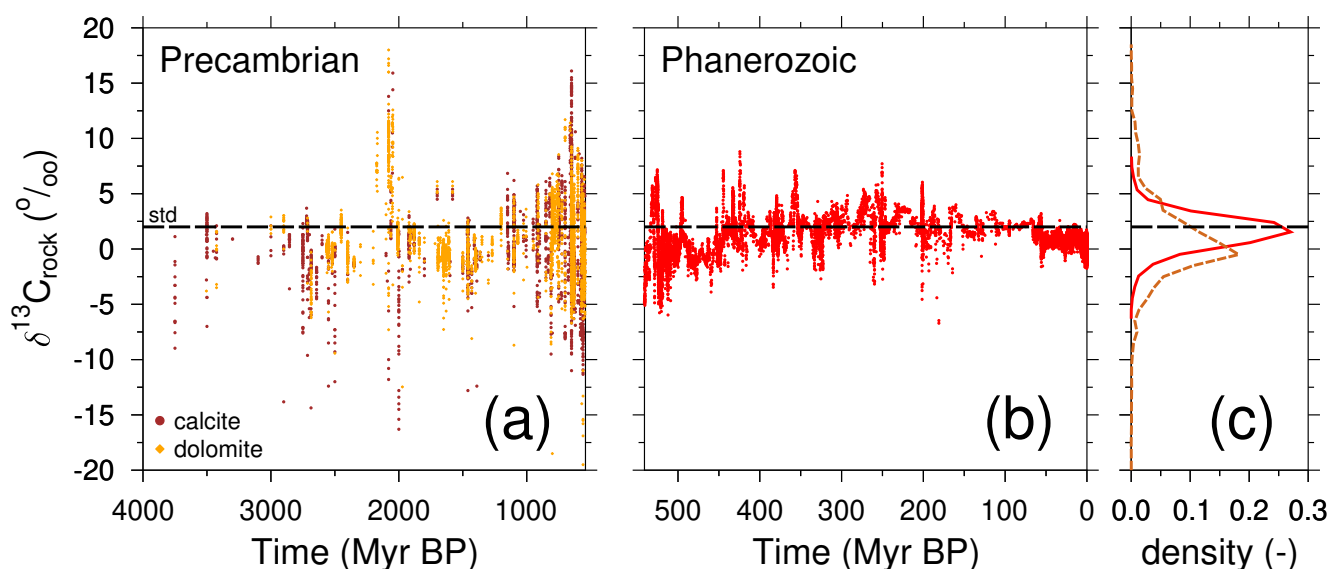
Figure 2. The δ^{13}C from carbonate rock from Earth's history. (a) Precambrian values of δ^{13}C calcite and dolomite rock as compiled in Prokoph et al. (2008). (b) Phanerozoic values as compiled in Bachan et al. (2017). (c) Normalised density plot of δ^{13}C data (broken line: Precambrian; solid line: Phanerozoic). The standard (std) parameter value of δ^{13}C$_{rock}$ = 2.0‰ used in the BICYCLE-SE model is also marked.

whole rock δ^{13}C isotope data for limestone and dolomite for the Precambrian (Fig. 2a), contains a huge scatter from –10 to +10‰ with a few excursions up to ±20‰ (Prokoph et al., 2008).

Calculated density distributions of these time series of δ^{13}C$_{rock}$ (Fig. 2c) are nearly normal distributed for the Phanerozoic with its mode being slightly lower (mean±σ = +1.5 ± 1.6‰) than the chosen standard parameter values of δ^{13}C$_{rock}$ = +2‰

120 in the BICYCLE-SE model (see section 2.2.1). Here, data have been interpolated to 10-yr equidistances before analysis. Data from the Precambrian have much larger gaps than for the Phanerozoic, which is why interpolation have not been applied. The distribution of the Precambrian δ^{13}C$_{rock}$, combining both calcite and dolomite, is more widely than for the Phanerozoic with a small mean value (+0.7 ± 3.6‰).

2.1.4 The δ^{13}C signature of volcanic CO$_2$

125 In BICYCLE-SE a δ^{13}C of −5‰ of volcanic CO$_2$ emissions (δ^{13}C$_v$) has been assumed, agreeing with a typical end member value from mantle material (Deines, 2002). However, reconstructions of δ^{13}C$_v$ are only available for a few sampled present day volcanoes, which nevertheless cover a wide range. For example, de Leeuw et al. (2007) found δ^{13}C$_v$ to vary between −2‰ and −12‰ in Honduras. At Baja California a range between −19‰ and −5‰ has been measured (Batista Cruz et al., 2019; Barry et al., 2020). Chiodini et al. (2011) detected for the Etna a positive trend in δ^{13}C$_v$, rising from −4‰ to −1‰ within 3–4

130 decades of the recent past.

2.2 Model

2.2.1 The carbon cycle box model BICYCLE-SE

The carbon cycle box model BICYCLE-SE has been fully described in Köhler and Munhoven (2020) with its ^{13}C cycle recently being updated (Köhler and Mulitza, 2024). This model version has recently been used to show that simulated changes in the

135 radiocarbon age of the ocean between the LGM and preindustrial times agree resonable well with reconstructions, although on millennial timescales (ignored here) abrupt changes in ocean circulation related to the bipolar seesaw need to be considered to meet deep ocean ^{14}C data (Köhler et al., 2024). Briefly, the BICYCLE core of the model consists of 10 ocean boxes, seven boxes for terrestrial carbon pools and a one-box atmosphere. Carbon and the carbon isotopes (and alkalinity, O_2 and PO_4^{3-} in the ocean) are calculated state variables of the model with explicitly considered carbonate chemistry in the ocean that distributes

140 DIC as function of temperature, salinity and pressure into its three chemical species (CO_2, HCO_3^-, CO_3^{2-}). In its update to a solid Earth (SE) version the model now contains a process-based sediment module that calculates, depending on carbonate chemistry, either the accumulation or the dissolution of $CaCO_3$ in the deep ocean and the shallow water loss of $CaCO_3$ due to coral reefs growth, simplistically calculated as function chemistry and sea level change. Furthermore, carbonate and silicate weathering introduce, either constantly or as function of atmospheric CO_2, a flux of bicarbonate (changing the total amount of

145 both carbon and alkalinity) into the surface ocean. Volcanic CO_2 outgassing on land as function of changing land ice volume, or from island and hot spot volcanoes as function of sea level change are other external carbon sources to the model. More details are found in the earlier papers describing the model.

Isotopic fractionation occurs mainly during gas exchange and biological production on land and in the ocean. The sizes of the corresponding fractionations in the ε-notation (in ‰) are summarised in Figure S2. Furthermore, the isotopic signatures

150 of the external inputs of carbon in the simulated system — of the weathered carbonate rock ($\delta^{13}C_{rock} = +2‰$) and of the volcanic CO_2 ($\delta^{13}C_v = -5‰$) — are necessary parameters of the model, which so far have been constantly prescribed by the mentioned values.

Climate change (ocean circulation, temperature, sea level and sea ice, aeolian iron input) influencing the marine carbon pumps and land carbon storage is prescribed externally from reconstructions. I here use different setups, either covering the

155 800-kyr long time window with ice core data (Köhler and Munhoven, 2020) or the last 5 Myr with most of the Plio-Pleistocene (Köhler, 2023). Forcing details were described in the relevant studies, but are summarised in the Figures S3–S4.

In the model geometry all of the Indo-Pacific Ocean below 1 km depth is combined in one box called deep Indo-Pacific. All the relevant deep ocean $\delta^{13}C$ data to which I compare my simulation results come from the deep Pacific. I always refer to either of these two elements when talking about the deep (Indo-)Pacific.

2.2.2 Reducing the model-data offset in the ^{13}C cycle

160

Various applications have shown that the model seems to be able to simulate G-IG changes in the carbon cycle in reasonable agreement with various paleo data (atmospheric CO_2, deep ocean CO_3^{2-}, surface ocean pH, deep ocean ^{14}C) (e.g. Köhler and Munhoven, 2020; Köhler, 2023; Köhler et al., 2024) while the long-term changes in $\delta^{13}C$ as found in the reconstructions are

so far not contained in a satifactory manner in the model output (e.g. Köhler and Bintanja, 2008; Köhler et al., 2010; Köhler

165 and Mulitza, 2024). Instead of searching for solutions which satisfy equally well the data constraints given by the carbon cycle itself and its stable carbon isotope I here follow a different approach. I take the main carbon cycle including simulated atmospheric CO_2 as given and analyse how changes in the isotopic signatures of the external input of carbon in the simulated system need to vary to align the simulated ^{13}C cycle, especially on orbital time scales, with data. In doing so I come to one possible realisation of how the carbon cycle might have changed in the past, which reasonably well agrees with reconstructions

170 of atmospheric carbon records (CO_2 and $\delta^{13}CO_2$) and marine $\delta^{13}C$, but I cannot exclude that other solutions might exist. Note, that the long-term effect of changes in the weathering flux strength, not its isotopic signature, on the ^{13}C cycle has recently been investigated with step-changes in the Bern3D model (Jeltsch-Thömmes and Joos, 2023).

For that effort I apply additional constraints to the model. I overwrite (or prescribe) one internally calculated variable of the ^{13}C cycle with reconstructions. This would in principle violate mass conservation of ^{13}C, but not if all necessary changes

175 can be explained by variations in $\delta^{13}C_{rock}$ or $\delta^{13}C_v$, the isotopic signatures of the geological sources. In a post-processing analysis I determine their necessary values from model-internal information as described in the following. Initial results already informed me that when prescribing $\delta^{13}CO_2$ the necessary anomalies in isotopic signatures of the external carbon sources need to be a lot bigger than the reconstructed ranges. In an alternative approach I therefore only weakly nudge the simulated $\delta^{13}C$ variable to its reconstruction. This approach can be used to check on necessary changes in either $\delta^{13}C_{rock}$ or $\delta^{13}C_v$ to align

180 simulations with reconstructions. Both constraints (prescribing or nudging) are applied to either atmospheric $\delta^{13}CO_2$ or to deep Indo-Pacific $\delta^{13}C$.

In detail, this approach works as follow: For each year t the data would ask for a change $\Delta(t)$ (in units of ‰ per year) in one variable of the model ($\delta^{13}C_{model}(t)$), e.g.

$$\Delta(t) = (\delta^{13}C_{data}(t) - \delta^{13}C_{model}(t)). \tag{1}$$

185 The difference of this data-model offset $\Delta(t)$ to the internally calculated change in this variable $\frac{\delta}{\delta t}(\delta^{13}C_{model}^{internal}(t))$, weighted by the nudging strength $\eta \in [0, 1]$, is the applied correction $\Delta_{cor}(t)$:

$$\Delta_{cor}(t) = \eta \cdot \left(\Delta(t) - \frac{\delta}{\delta t}(\delta^{13}C_{model}^{internal}(t)) \right), \tag{2}$$

that is added to the differential equation

$$\frac{\delta}{\delta t}(\delta^{13}C_{model}^{final}(t)) = \frac{\delta}{\delta t}(\delta^{13}C_{model}^{internal}(t)) + \Delta_{cor}(t). \tag{3}$$

190 If $\eta = 1$ these equations simplify to

$$\frac{\delta}{\delta t}(\delta^{13}C_{model}^{final}(t)) = \Delta(t) \tag{4}$$

and the approach describes the prescription of $\delta^{13}C$ with data. In other words, prescription is the most extreme case of nudging.

In the post-processing it is calculated how $\Delta_{cor}(t)$ can be caused by changes in the isotopic signature of the external sources to the simulated carbon cycle. Thus, the following hypothetical isotopic signatures for the external fluxes are calculated:

195 $$\delta^{13}C_{rock}^{hypo}(t) = \frac{C(t)}{0.5 \cdot f_{wCa}(t)} \cdot \Delta_{cor}(t) + \delta^{13}C_{rock}^{std} \tag{5}$$

and

$$\delta^{13}C_v^{hypo}(t) = \frac{C(t)}{f_v(t)} \cdot \Delta_{cor}(t) + \delta^{13}C_v^{std} \tag{6}$$

Here, $C(t)$ is the amount of carbon (in units gC) at time t in the atmosphere, when nudging to atmospheric $\delta^{13}CO_2$, or in the deep Indo-Pacific ocean box, when nudging to deep Indo-Pacific $\delta^{13}C$ with $f_{wCa}(t)$ and $f_v(t)$ being the annual fluxes
200 (in units of gC per year) of carbonate weathering and volcanic outgassing, respectively. The factor 0.5 in the denominator in Equation 5 acknowledges that only half of the carbon in carbonate weathering has its source in weathered rock (e.g. Hartmann et al., 2009). In my 800-kyr long simulations f_{wCa} is constant at 12 TmolC/yr (0.144 PgC/yr), while it varies as function of CO_2 between 10–15 Tmol/yr (0.12–0.18 PgC/yr) during the multi-millions year long runs. The volcanic CO_2 outgassing flux ($f_v(t) \sim$5–16 Tmol/yr or 0.06–0.192 PgC/yr) is a by 4-kyr time-delayed function of sea level change.

205 I determined the strength $\eta_{DP} = 0.0001$ when nudging to deep Indo-Pacific $\delta^{13}C$ by comparing the resulting width of the distribution in $\delta^{13}C_{rock}^{hypo}(t)$ to the reconstructions (Figure 2c). A comparable strength of the nudging is inversely related to the amount of carbon in the relevant box. From the about 30 times more carbon in the deep Indo-Pacific box than in the atmosphere, it was infered that $\eta_A = \eta_{DP} \cdot 30 = 0.003$. For reasons of simplicity and due to a lack of data which would allow to calculate a distribution of $\delta^{13}C_v$ the same nudging strength is used when calculating $\delta^{13}C_v^{hypo}(t)$.

210 In my setup all CO_2 from volcanic outgassing is directly released into the atmosphere. It has been shown (Hasenclever et al., 2017) that submarine and subaerial injections of volcanic CO_2 lead to similar changes in the carbon cycle on multi-millennial time scale making a distinction of volcanism in the two subgroups irrelevant here. Important for long-term CO_2 is the amount of added carbon to the atmosphere-ocean-biosphere system, not the location of the injection. This is also the reason why I investigate (a) how changes in $\delta^{13}C_{rock}$, which as part of weathering (or of bicarbonate injection) enters the system in the
215 surface ocean, might have an influence on atmospheric $\delta^{13}CO_2$, and (b) how both weathering and volcanism might change deep ocean $\delta^{13}C$. Furthermore, these insights also suggest, that for cases of very strong nudging, as found in the prescribing scenarios, results can probably not be explained by isotopic signature changes of the external carbon fluxes.

As final check for my hypothesis that the long-term changes in $\delta^{13}C$ might be caused by the isotopic signature of the external sources to the carbon cycle I compared $\delta^{13}C$ from nudging scenarios with simulations in which either $\delta^{13}C_{rock}^{hypo}(t)$ or
220 $\delta^{13}C_v^{hypo}(t)$ as derived from Equations 5–6 is externally prescribed (Figure S5). Differences between both setup are generally less than 0.02‰ in various variables of the ^{13}C cycle for the last 800 kyr supporting my post-processing approach to reliably calculate the necessary isotopic signatures of these two fluxes in order to reduce the model-data offset in the ^{13}C cycle.

2.2.3 Scenarios

My standard run (SEi) is based on the 800-kyr long scenario SE in Köhler and Munhoven (2020) with updates, mainly in
225 the ^{13}C cycle, as described in Köhler and Mulitza (2024). Prescribing, or nudging to, atmospheric $\delta^{13}CO_2$ (Eggleston et al., 2016) is performed in scenarios C1 or C2, respectively. Here, simulations are started at 210 kyr BP in the interglacial around MIS7a-c and the value of $\delta^{13}CO_2$ before 155 kyr is assumed to stay constant. The whole 800-kyr long runs are alternatively prescribed with (D1), or nudged to (D2), the deep Pacific $\delta^{13}C$ stack. For an even longer perspective I rely on the 5 Myr-long

Table 1. Summery of applied simulation scenarios. The column "control" marks with "yes" the control runs or names the related controls.

Name	Length	Control	Description
SEi	800 kyr	yes	The control run SE from Köhler and Munhoven (2020) with updated ^{13}C cycle (Köhler and Mulitza, 2024)
C1	210 kyr	SEi	Atmospheric $\delta^{13}CO_2$ are **prescribed** from data
C2	210 kyr	SEi	Atmospheric $\delta^{13}CO_2$ are **nudged** to data
D1	800 kyr	SEi	Deep Indo-Pacific ocean δ^{13}C are **prescribed** from the 6-cores stack
D2	800 kyr	SEi	Deep Indo-Pacific ocean δ^{13}C are **nudged** to the 6-cores stack
SEi++V6	5 Myr	yes	The 5 Myr-long run SE++V6 from Köhler (2023) with strong weathering and 6% decline in volcanic outgassing 4–1 Myr with updated ^{13}C cycle (Köhler and Mulitza, 2024)
D1-L	5 Myr	SEi++V6	Deep Indo-Pacific ocean δ^{13}C are **prescribed** from the 6-cores stack
D2-L	5 Myr	SEi++V6	Deep Indo-Pacific ocean δ^{13}C are **nudged** to the 6-cores stack
D2-P	5 Myr	SEi++V6	Deep Indo-Pacific ocean δ^{13}C are **nudged** to the 5-points running mean δ^{13}C from ODP846

runs published in Köhler (2023). Here, I choose a scenario based on run SE++V6, in which weathering is strongly coupled
230 to atmospheric CO_2 and volcanic outgassing is decreasing by 6% between 4 and 1 Myr BP leading to a gradual decline in
atmospheric CO_2. Tests have shown that the findings I describe further below are also robust for other scenarios included in
Köhler (2023) with different weathering strength and volcanic history leading to alternative atmospheric CO_2 time series. Even
when forced with the new 4.5 Myr long compilation of changes in surface temperature (Clark et al., 2024), which contains
some power in periodicities slower than 100-kyr, my conclusions stay the same. I distinguish between a control run (SEi++V6),
235 3-Myr long runs in which deep Indo-Pacific δ^{13}C is either prescribed with (D1-L) or nudged to (D2-L) the δ^{13}C stack, and a
5-Myr long run (D2-P) nudged to δ^{13}C in ODP846. An overview on all scenarios is compiled in Table 1.

2.3 Analysis tools

I use R (R Core Team, 2023) for calculating wavelets with WaveletComp (Roesch and Schmidbauer, 2018) and for further
frequency analysis including coherence the package seewave, version 2.2.3. In all wavelet figures the white lines mark the 0.1
240 significant level and the yellow lines the ridges of the power distribution. Detrending of data has been performed with Matlab
(The MathWorks Inc., 2023).

3 Results

Atmospheric CO_2 as simulated in my scenarios is shown as control (Figure 3, first row) against data (Bereiter et al., 2015).
This is chosen here as an indicator of the dynamics of the carbon cycle whose in depth discussions are covered in previous
245 papers (Köhler and Munhoven, 2020; Köhler, 2023).

Simulations without prescription or nudging to δ^{13}C contain during the late Pleistocene typical multi-millennial variations of the order of 0.5‰ in atmospheric δ^{13}CO$_2$ (Figure 3, second row), of 0.3‰ in δ^{13}C$_{\rm DIC}$ of the wider tropical surface ocean (Figure 3, third row), and of G/IG variations of 0.5‰ in δ^{13}C$_{\rm DIC}$ of the deep Indo-Pacific (Figures 3, fourth row). As shown before (Köhler and Mulitza, 2024) atmospheric δ^{13}CO$_2$ and δ^{13}C$_{\rm DIC}$ of the wider tropical surface ocean are on

250   orbital timescales of 41-kyr periodicities highly correlated. In scenarios C1 (prescribed δ^{13}CO$_2$) and C2 (nudged to δ^{13}CO$_2$) there is also a loose correlation between atmospheric δ^{13}CO$_2$ and deep Indo-Pacific δ^{13}C on these timescales (Figure S6) with a coherence that rose from below 0.2 in scenario SEi to 0.6 (C1) or 0.4 (C2). A tighter correlation between δ^{13}C in the deep ocean and the atmosphere is not expected since the marine carbon pumps introduce vertical gradients in δ^{13}C (e.g. Schmittner et al., 2013) with opposite effects on atmospheric δ^{13}CO$_2$ (or surface ocean δ^{13}C) and deep ocean δ^{13}C on G-IG timescales

255   (Köhler et al., 2010). Therefore, there has to be a certain anticorrelation between atmospheric δ^{13}CO$_2$ / surface ocean δ^{13}C on the one hand and deep Pacific δ^{13}C on the other hand. In other words, prescribing or nudging to atmospheric δ^{13}CO$_2$ or deep Pacific δ^{13}C always also increases the agreement of the simulations to the reconstructions in the other variable, but a perfect fit in the other endmember of the ^{13}C cycle is not expected. In scenarios C2 and D2 the long-term evolution from PGM-to-LGM in both atmospheric δ^{13}CO$_2$ and wider surface ocean δ^{13}C is covered in the simulations, but the local maxima in the

260   data around 80 kyr BP is not contained, suggesting that not these solid Earth fluxes but internal processes in the atmosphere-ocean-biosphere subsystem are responsible for these anomalies, which occur on shorter timescales. Millennial-scale changes in atmospheric δ^{13}CO$_2$ between 70 and 60 kyr BP have already been successfully explained by such internal processes (Menking et al., 2022), which were probably also active around 80 kyr BP.

The introduction of the long-term periodicities into my simulated ^{13}C cycle can be seen in the spectral analysis. Wavelets

265   show — apart from the time window 4–3 Myr BP — no power in periodicities beyond 100-kyr in the deep Indo-Pacific δ^{13}C in the control simulations SEi and SEi++V6 (Figure 4a,b), but simulations contain power comparable to the data around 400-kyr but also in 200-kyr periodicities when nudged to the reconstructions (Figures 1c,d and 4c,d). I therefore conclude that on these slow timescales my nudged simulations are in reasonable agreement with the data.

The distributions of δ^{13}C$_{\rm rock}^{\rm hypo}$ or of δ^{13}C$_{\rm v}^{\rm hypo}$ necessary the close the ^{13}C cycle in the long eccentricity timescale are for the

270   different scenarios together with the data constraints compiled in Figure 5. When prescribing one δ^{13}C record from data (scenarios C1, D1, D1-L), it is clearly seen that the necessary distributions of the parameter values are with $1\sigma > 14$‰ (δ^{13}C$_{\rm rock}^{\rm hypo}$) and $1\sigma > 9$‰ (δ^{13}C$_{\rm v}^{\rm hypo}$) much wider than what reconstructions are suggesting (e.g. $1\sigma < 4$‰ for δ^{13}C$_{\rm rock}$). This finding indicates, that a prescription of δ^{13}C, during which the model would follow the reconstruction not only on orbital timescales, but also during shorter multi-millennia anomalies, cannot be explained by the isotopic signature of either carbonate rock or

275   volcanic outgassing.

The nudged 800-kyr long simulations well overlap with the Phanerozoic reconstructions of δ^{13}C in carbonate rock (D2: 0.8$\pm$3.0‰), while in longer simulations I find even tighter distributions, but with lower mean values (D2-L: 0.2$\pm$2.6‰; D2-P: –0.4$\pm$3.0‰) more in agreement with the Precambrian δ^{13}C rock data. Similarly, the mean in δ^{13}C$_{\rm v}^{\rm hypo}$ is lower in nudged multi-millions years simulations than in those covering only 800-kyr (D2: –5.1$\pm$2.0‰; D2-L: –6.2$\pm$1.7‰; D2-P: –6.6$\pm$2.0‰)

280   and the distribution are with $1\sigma \leq 2$‰ sufficiently narrow and overlap with data of δ^{13}C in volcanic CO$_2$. Remember, that the

nudging strength η_{DP} was determined from the width of the distribution of $\delta^{13}\mathrm{C_{rock}^{hypo}}$ in scenario D2 to be comparable to the data, but its mean value was never used as tuning target, it freely evolved from the simulations and the post-processing analysis. The shift towards lower mean values in $\delta^{13}\mathrm{C_{rock}^{hypo}}$ or $\delta^{13}\mathrm{C_v^{hypo}}$ for longer simulations is dominantly caused by $\delta^{13}\mathrm{C}$ in ODP846 (used for nudging in scenario D2-P) being on average lower than $\delta^{13}\mathrm{C}$ in the deep Pacific stack (used for nudging in scenarios 285 D2 and D2-L).

When nudged to $\delta^{13}\mathrm{CO_2}$ (scenario C2) I obtain a rather skewed distribution of $\delta^{13}\mathrm{C_{rock}^{hypo}}$ ($2.7 \pm 2.6‰$) which is wider than the reconstruction from carbonate rock (Figure 5a). The width of the solution is not improving if I revise the nudging strength η_A within reasonable bounds. Thus, it seems that the shortness of the $\delta^{13}\mathrm{CO_2}$ time series, which covers not even half of one long eccentricity cycle is responsible for this unsatisfactory result. The distribution for $\delta^{13}\mathrm{C_v^{hypo}}$ ($-4.5 \pm 1.7‰$) in scenario C2 290 is in its width not a lot different from what I obtain in scenario D2 from longer runs and nudging to deep Pacific $\delta^{13}\mathrm{C}$, but the shape of the distribution is without a clear maximum well different from a bell-shaped Gaussian curve of a normal distribution (Figure 5c). Starting this analysis initially from understanding $\delta^{13}\mathrm{CO_2}$ the available data are not yet covering a sufficiently long period for a complete understanding of the 405-kyr cycle in them.

As side effect, my nudging approach also increases the G-IG amplitudes in the simulated $^{13}\mathrm{C}$ cycle in the pre-MPT times. In 295 the data and in the prescribed scenario D1-L the G-IG amplitudes in deep Indo-Pacific $\delta^{13}\mathrm{C}$ have prior to the MPT only been reduced to 75% of their post-MPT size, while in the control run SEi++V6 they have been reduced to 24% (Figures 1a, 3c). My nudging approach increases these pre-MPT G-IG amplitudes to 41% (D2-L) and 32% (D2-P) of their amplitudes during the last 1 Myr, thus partially explaining this feature of the 41-kyr world (Figure 3c).

All-together I conclude, that indeed both the carbon isotopic signature of either carbonate rocks or of volcanic $\mathrm{CO_2}$ out- 300 gassing might be the process which closes the $^{13}\mathrm{C}$ cycle on periodicities slower than 100-kyr in the Plio-Pleistocene. Further-more, the PGM-to-LGM offset in atmospheric $\delta^{13}\mathrm{CO_2}$ and the long eccentricity in benthic $\delta^{13}\mathrm{C}$ are potentially caused by the same processes and are therefore related to each other.
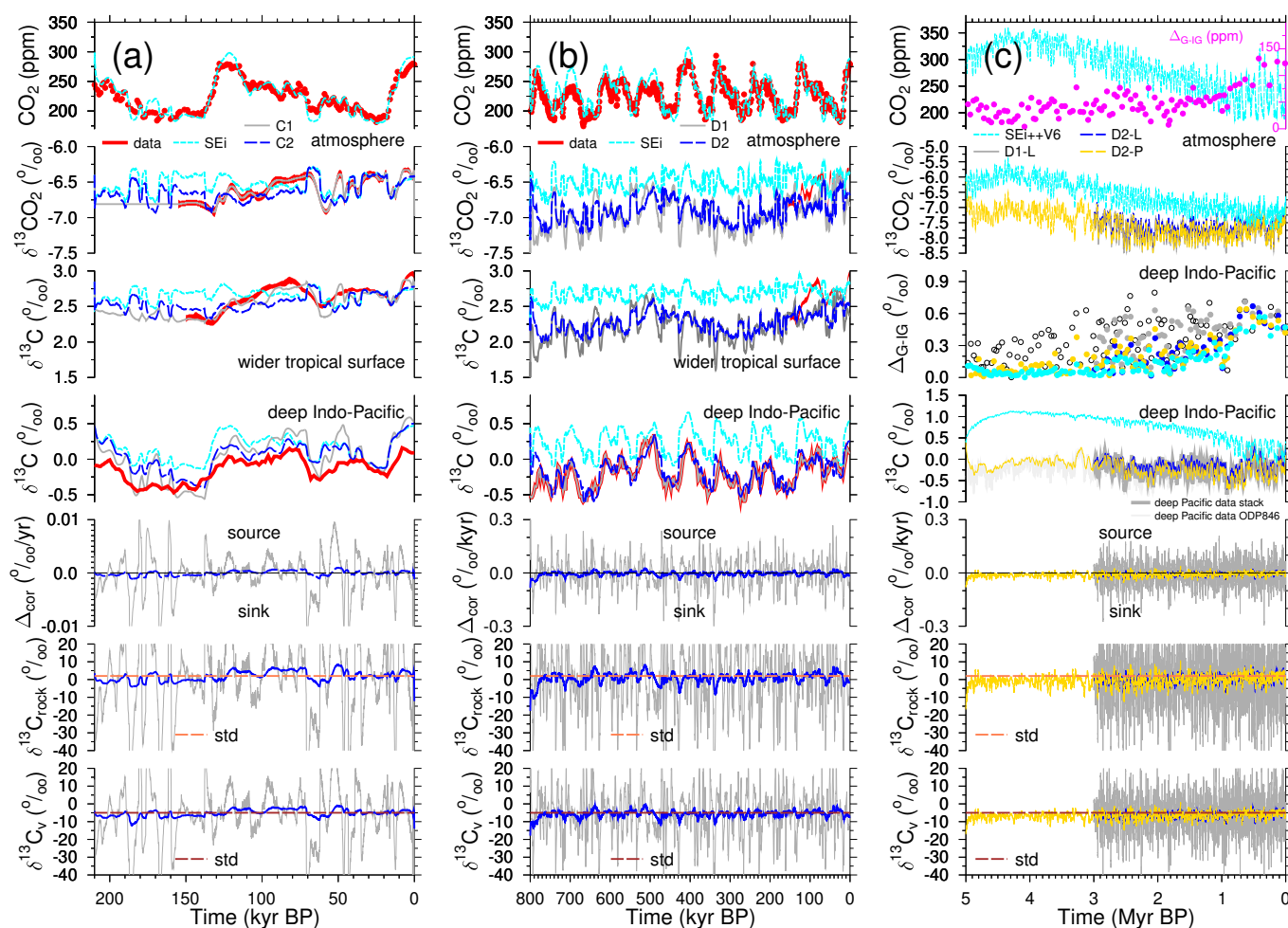
Figure 3. Closure of the ^{13}C cycle on 405-kyr periodicity. From top-to-bottom: Atmospheric CO_2, $\delta^{13}CO_2$, $\delta^{13}C$ in DIC of surface water of the wider tropics, or in the deep Indo-Pacific, Δ_{cor}, $\delta^{13}C_{rock}^{hypo}$, $\delta^{13}C_v^{hypo}$ for different scenarios including reconstructions of CO_2 (Bereiter et al., 2015), $\delta^{13}CO_2$ (Eggleston et al., 2016), $\delta^{13}C_{DIC}$ in the surface ocean of the wider tropics (anomalies to the LGM in the mono-specific stack of *G. ruber*, $\Delta(\delta^{13}C_{rub})$ from Köhler and Mulitza (2024)) or in the deep Pacific from the 6 cores stack (Lisiecki, 2014) or ODP846 (Poore et al., 2006). Δ_{cor} is calculated from (a) atmospheric $\delta^{13}CO_2$ or (b, c) from deep Indo-Pacific $\delta^{13}C$. In (c) Δ_{G-IG} are included for CO_2 (first row, right y-axis) and deep Indo-Pacific $\delta^{13}C$ including in open black circles those for ODP846 (third row), but no $\delta^{13}C$ in DIC of the wider tropical surface ocean. For Δ_{G-IG} the difference between a glacial minima and the subsequent interglacial maxima are calculated following the MIS boundary definition of Lisiecki and Raymo (2005) with points being positioned at mid-transitions.
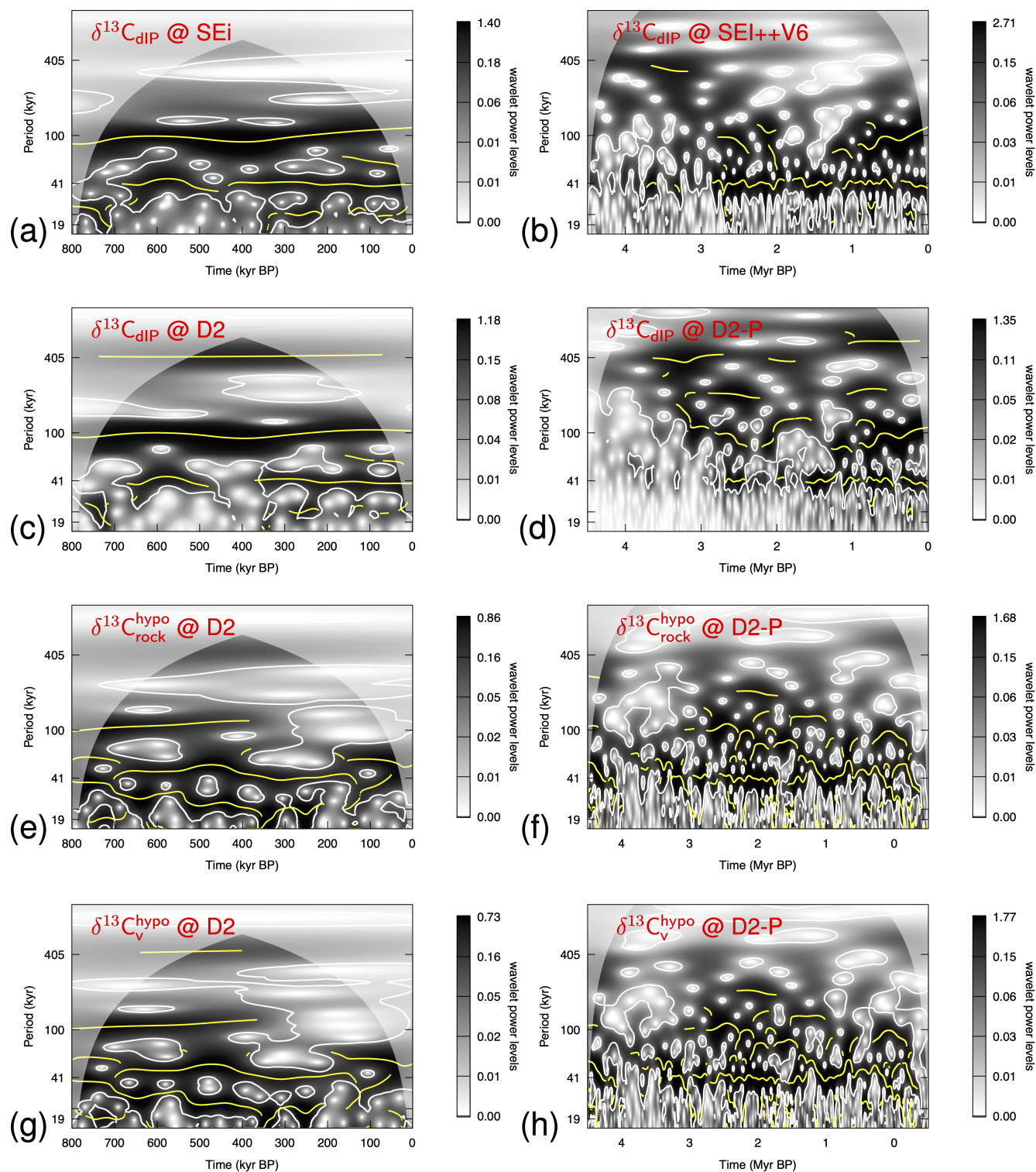
Figure 4. Wavelets of either the deep Indo-Pacific $\delta^{13}C$ in (a–d) or of my solution for (e,f) $\delta^{13}C_{rock}^{hypo}$ and (g,h) $\delta^{13}C_{v}^{hypo}$ for different scenarios (left: SEi-D2 or D2; right: SEi++V6 or D2-P). Results are restricted to the last 4.5 Myr to avoid long spinup effects and only data in panel b have been detrended before spectral analysis.
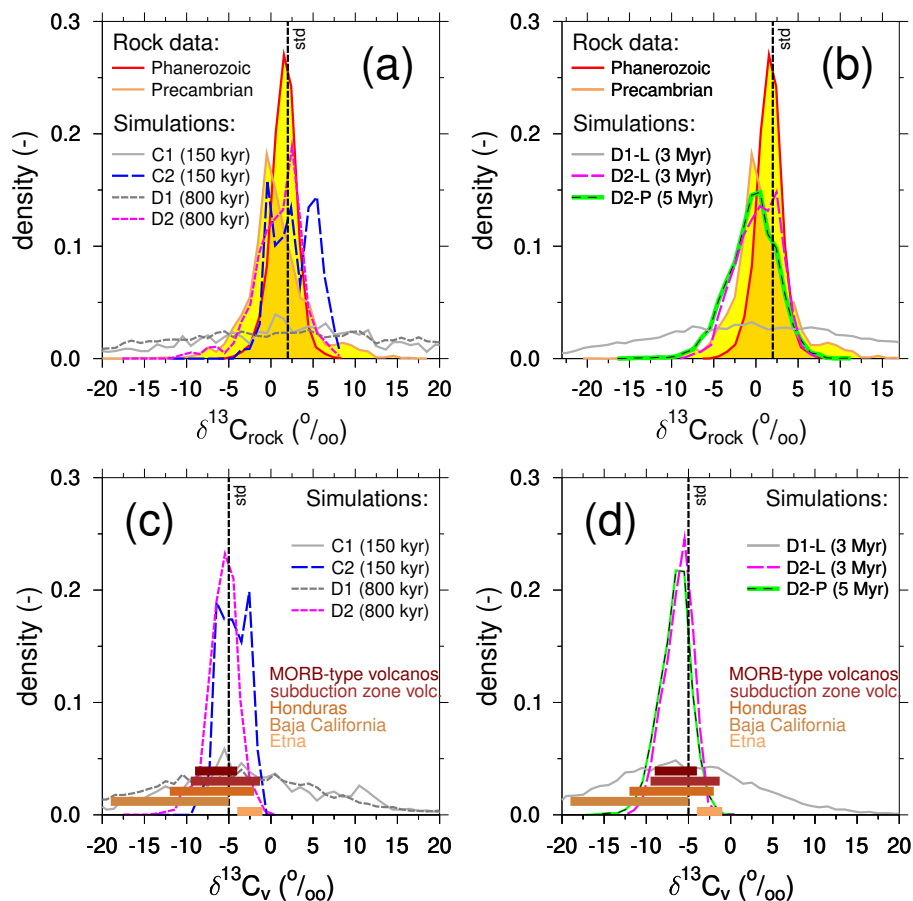
Figure 5. Distribution of carbon isotopic signature of (a, b) carbonate rock ($\delta^{13}C_{rock}$) and of (c, d) volcanic CO_2 ($\delta^{13}C_v$) from Earth's history in data and simulations. More details on the rock data are found in Figure 2. Up to 800-kyr long simulations (a, c) versus multi-million years long simulations (b, d). The reconstructions of $\delta^{13}C_v$ in (c, d) have no density information, but only the observed ranges (colour-coded to the different studies) are sketched. MORB: mid-ocean ridge basalt. Sources for $\delta^{13}C_v$: MORB-type and subduction zone volcanoes (Sano and Williams, 1996); Honduras (de Leeuw et al., 2007); Baja California (Batista Cruz et al., 2019; Barry et al., 2020); Etna (Chiodini et al., 2011).

4 Discussions

A frequency analysis of the derived solutions for $\delta^{13}C_{\mathrm{rock}}^{\mathrm{hypo}}$ and $\delta^{13}C_{\mathrm{v}}^{\mathrm{hypo}}$ (Figure 4e–h) finds that only little power is contained
305 in periodicities beyond 100-kyr. Results for both variables are dominated by power in the obliquity band and some contributions
to the 100-kyr band. Between 2–3 Myr BP some enhanced power in the 200-kyr periods is contained in both solutions obtained
from scenario D2-P. Modifications in either $\delta^{13}C_{\mathrm{rock}}^{\mathrm{hypo}}$ or $\delta^{13}C_{\mathrm{v}}^{\mathrm{hypo}}$, both rather powerless around 405-kyr, lead nevertheless
to a persisting occurrence of the long eccentricity in the resulting ^{13}C cycle. A transition of power to other frequencies was
suggested to be caused by the long residence time of carbon in the ocean during earlier quasi ice-free periods of the Cenozoic
310 (Pälike et al., 2006; Zeebe et al., 2017). However, the power transition here had probably other reasons since the main carbon
cycle and CO_2 contain no power in 405-kyr periodicity (Figure S1g–i), which was not the case in these other studies. Remember
that in non-linear systems resulting frequencies might differ from those in the forcing (e.g. Rial et al., 2004).

Obliquity has an influence on incoming solar radiation in the high latitudes and is therefore thought to be the main control
for land ice dynamics in the northern hemisphere (e.g. Huybers, 2007; Willeit et al., 2019; Köhler and van de Wal, 2020). Thus,
315 obliquity together with some influence of precession (Huybers, 2011) and internal feedbacks (e.g. Willeit et al., 2019; Berends
et al., 2021; Clark et al., 2024) determines the G-IG cyclicity of the Plio-Pleistocene. Therefore, the dominance of obliquity in
my solutions for either $\delta^{13}C_{\mathrm{rock}}^{\mathrm{hypo}}$ or $\delta^{13}C_{\mathrm{v}}^{\mathrm{hypo}}$ suggests that land ice might also play an important role in my closure of the ^{13}C
cycle for slow timescales of the Plio-Pleistocene.

Previously, the Pleistocene 400–500 kyr periodicity in marine $\delta^{13}C$ has been suggested to be caused by continental weath-
320 ering and monsoon activity (Wang et al., 2010, 2014) and climate simulations also highlight the role of the 405-kyr periodicity
on tropical precipitation (Yun et al., 2023). The Asia monsoon during the last 650 kyr as deduced from detrended $\delta^{18}O$ in
speleothems has significant power in obliquity, but in antiphase to summer insolation at 65°N, which suggests that the ultimate
cause for the 41-kyr-related changes are situated in the northern hemispheric ice sheets (Cheng et al., 2016). Furthermore,
present-day reconstructions of the continental weathering rates indicate that highly active regions dominate the global signal
325 with 10% of the area contributing about 50% of the global weathering fluxes (Hartmann et al., 2009). I therefore suggest that
obliquity-driven changes might also easily control weathering strength of different areas, finally ending in changes in $\delta^{13}C_{\mathrm{rock}}^{\mathrm{hypo}}$
without the need for large variations in the global weathering flux itself. This influence of obliquity might operate via monsoon,
but also a variable contribution of available weatherable rock around dynamic ice sheets in North America and Eurasia or from
continental shelves during sea level low stands seems possible (e.g. Börker et al., 2020).
330 Dominant power in the obliquity band is also contained in reconstructed volcanism from the ring of fire during the last 1 Myr
(Kutterolf et al., 2013). In a revised analysis this power in 41-kyr is reduced and only second behind 100-kyr (Kutterolf et al.,
2019). This spectral analysis supports hypotheses that either changes in land ice load or in sea level might influence subaerial or
submarine volcanism, respectively (Huybers and Langmuir, 2009, 2017; Hasenclever et al., 2017). Obliquity-related changes
in $\delta^{13}C_{\mathrm{v}}^{\mathrm{hypo}}$ as deduced here are therefore also easily conceivable.

5 Conclusions

Taken together my analysis suggests that variations in the isotopic signatures of the geological sources (δ^{13}C of weathered carbonate rock or δ^{13}C of volcanic outgassed CO_2) might without any further changes in the carbon cycle be sufficient to explain the signals in δ^{13}C related to the long eccentricity cycle during most of the Plio-Pleistocene. Furthermore, my suggested solution connects this periodicity around the 405-kyr in deep ocean δ^{13}C with the PGM-to-LGM offset in atmospheric $\delta^{13}CO_2$ implying that both are caused by the same underlying processes. My analysis highlights the influence of obliquity on these changes in the ^{13}C cycle, which I interpret as northern hemispheric ice sheets being the ultimate cause for the necessary variations in $\delta^{13}C_{\mathrm{rock}}$ or $\delta^{13}C_{\mathrm{v}}$. Studies show that both weathering and volcanic activity might, directly or indirectly, be influenced by land ice dynamics giving independent support for my hypothesis. Taken the link to obliquity as granted it is furthermore unlikely that the same mechanisms might have been responsible for the 405-kyr periodicity in marine δ^{13}C found in earlier climates of the Cenozoic since there has not been any substantial northern hemisphere ice sheet (Pälike et al., 2006; Zeebe et al., 2017; De Vleeschouwer et al., 2020; Westerhold et al., 2020). During these times not only δ^{13}C, but also δ^{18}O and potentially atmospheric CO_2 contained cyclicity related to the long eccentricity which is missing here for the Plio-Pleistocene, also asking for other solutions to the problem. However, both my possible answers, either via carbonate weathering or via volcanism, seems similarly likely. So far, I have not yet found a criteria which makes one more likely than the other, and probably a mixture of both is the most realistic solution to the here suggested closure of the ^{13}C cycle on these slow timescales. The dominance of obliquity in my solutions readily explains an improvement in simulated G-IG amplitudes in δ^{13}C in the 41-kyr world of the Plio-Pleistocene, but their reconstructed sizes are not fully obtained. Thus, while the influence of the isotopic signature of the geological sources might be important for the decoupling of climate from the carbon cycle there is room for other, not yet detected, processes for a complete understanding of the Plio-Pleistocene ^{13}C cycle.

Data availability. Simulation results data will be available from PANGAEA (registration pending). For the review process these data are accessible (1 zip-file <3 MB) under https://my.hidrive.com/lnk/EWhObJhSL.

Author contributions. Since this is a one-author study all has been performed by the single author (PK).

Competing interests. The author declares no competing interests.

Acknowledgements. I thank Richard Zeebe for pointing the work of Hilgen et al. (2020) on the 200-kyr cycle to me, P.U. Clark for some comments on earlier versions of the draft and Florian Krauss and Jochen Schmitt for some insights on $\delta^{13}CO_2$ derived from ice cores.

References

Ahn, S., Khider, D., Lisiecki, L. E., and Lawrence, C. E.: A probabilistic Pliocene-Pleistocene stack of benthic d18O using a profile hidden Markov model, Dynamics and Statistics of the Climate System, 2, dzx002, https://doi.org/10.1093/climsys/dzx002, 2017.

Bachan, A., Lau, K. V., Saltzman, M. R., Thomas, E., Kump, L. R., and Payne, J. L.: A model for the decrease in amplitude of carbon isotope excursions across the Phanerozoic, American Journal of Science, 317, 641–676, https://doi.org/10.2475/06.2017.01, 2017.

Barry, P. H., Negrete-Aranda, R., Spelz, R. M., Seltzer, A. M., Bekaert, D. V., Virrueta, C., and Kulongoski, J. T.: Volatile sources, sinks and pathways: A helium-carbon isotope study of Baja California fluids and gases, Chemical Geology, 550, 119 722, https://doi.org/10.1016/j.chemgeo.2020.119722, 2020.

Batista Cruz, R. Y., Rizzo, A. L., Grassa, F., Bernard Romero, R., González Fernández, A., Kretzschmar, T. G., and Gómez-Arias, E.: Mantle Degassing Through Continental Crust Triggered by Active Faults: The Case of the Baja California Peninsula, Mexico, Geochemistry, Geophysics, Geosystems, 20, 1912–1936, https://doi.org/10.1029/2018GC007987, 2019.

Bereiter, B., Eggleston, S., Schmitt, J., Nehrbass-Ahles, C., Stocker, T. F., Fischer, H., Kipfstuhl, S., and Chappellaz, J.: Revision of the EPICA Dome C CO_2 record from 800 to 600 kyr before present, Geophysical Research Letters, 42, 542–549, https://doi.org/10.1002/2014GL061957, 2015.

Berends, C. J., Köhler, P., Lourens, L. J., and van de Wal, R. S. W.: On the Cause of the Mid-Pleistocene Transition, Reviews of Geophysics, 59, e2020RG000 727, https://doi.org/10.1029/2020RG000727, 2021.

Börker, J., Hartmann, J., Amann, T., Romero-Mujalli, G., Moosdorf, N., and Jenkins, C.: Chemical weathering of loess during the Last Glacial Maximum, Mid-Holocene and today, Geochemistry, Geophysics, Geosystems, 21, e2020GC008 922, https://doi.org/10.1029/2020GC008922, 2020.

Cheng, H., Edwards, R. L., Sinha, A., Spötl, C., Yi, L., Chen, S., Kelly, M., Kathayat, G., Wang, X., Li, X., Kong, X., Wang, Y., Ning, Y., and Zhang, H.: The Asian monsoon over the past 640,000 years and ice age terminations, Nature, 534, 640–646, https://doi.org/10.1038/nature18591, 2016.

Chiodini, G., Caliro, S., Aiuppa, A., Avino, R., Granieri, D., Moretti, R., and Parello, F.: First $^{13}C/^{12}C$ isotopic characterisation of volcanic plume CO_2, Bulletin of Volcanology, 73, 531—542, https://doi.org/10.1007/s00445-010-0423-2, 2011.

Clark, P. U., Shakun, J. D., Rosenthal, Y., Köhler, P., and Bartlein, P. J.: Global and regional temperature change over the past 4.5 million years, Science, 383, 884–890, https://doi.org/10.1126/science.adi1908, 2024.

de Leeuw, G., Hilton, D., Fischer, T., and Walker, J.: The He-CO_2 isotope and relative abundance characteristics of geothermal fluids in El Salvador and Honduras: New constraints on volatile mass balance of the Central American Volcanic Arc, Earth and Planetary Science Letters, 258, 132 – 146, https://doi.org/10.1016/j.epsl.2007.03.028, 2007.

De Vleeschouwer, D., Drury, A. J., Vahlenkamp, M., Rochholz, F., Liebrand, D., and Pälike, H.: High-latitude biomes and rock weathering mediate climate–carbon cycle feedbacks on eccentricity timescales, Nature Communications, 11, 5013, https://doi.org/10.1038/s41467-020-18733-w, 2020.

Deines, P.: The carbon isotope geochemistry of mantle xenoliths, Earth-Science Reviews, 58, 247 – 278, https://doi.org/10.1016/S0012-8252(02)00064-8, 2002.

Eggleston, S., Schmitt, J., Bereiter, B., Schneider, R., and Fischer, H.: Evolution of the stable carbon isotope composition of atmospheric CO_2 over the last glacial cycle, Paleoceanography, 31, 434–452, https://doi.org/10.1002/2015PA002874, 2016.

Faccenna, C., Becker, T. W., Holt, A. F., and Brun, J. P.: Mountain building, mantle convection, and supercontinents: Holmes (1931) revisited, Earth and Planetary Science Letters, 564, 116 905, https://doi.org/10.1016/j.epsl.2021.116905, 2021.

Hartmann, J., Jansen, N., Dürr, H. H., Kempe, S., and Köhler, P.: Global CO_2-consumption by chemical weathering: What is the contribution of highly active weathering regions?, Global and Planetary Change, 69, 185–194, https://doi.org/10.1016/j.gloplacha.2009.07.007, 2009.

Hasenclever, J., Knorr, G., Rüpke, L., Köhler, P., Morgan, J., Garofalo, K., Barker, S., Lohmann, G., and Hall, I.: Sea level fall during glaciation stabilized atmospheric CO_2 by enhanced volcanic degassing, Nature Communications, 8, 15 867, https://doi.org/10.1038/ncomms15867, 2017.

Hilgen, F., Zeeden, C., and Laskar, J.: Paleoclimate records reveal elusive 200-kyr eccentricity cycle for the first time, Global and Planetary Change, 194, 103 296, https://doi.org/10.1016/j.gloplacha.2020.103296, 2020.

Huang, H., Gao, Y., Ma, C., Jones, M. M., Zeeden, C., Ibarra, D. E., Wu, H., and Wang, C.: Organic carbon burial is paced by a ∼173-ka obliquity cycle in the middle to high latitudes, Science Advances, 7, eabf9489, https://doi.org/10.1126/sciadv.abf9489, 2021.

Huybers, P.: Glacial variability over the last two million years: an extended depth-derived agemodel, continuous obliquity pacing, and the Pleistocene progression, Quaternary Science Reviews, 26, 37–55, https://doi.org/10.1016/j.quascirev.2006.07.013, 2007.

Huybers, P.: Combined obliquity and precession pacing of late Pleistocene deglaciations, Nature, 480, 229–232, https://doi.org/10.1038/nature10626, 2011.

Huybers, P. and Langmuir, C.: Feedback between deglaciation and volcanism, and atmospheric CO_2, Earth and Planetary Science Letters, 286, 479–491, https://doi.org/10.1016/j.epsl.2009.07.014, 2009.

Huybers, P. and Langmuir, C. H.: Delayed CO_2 emissions from mid-ocean ridge volcanism as a possible cause of late-Pleistocene glacial cycles, Earth and Planetary Science Letters, 457, 238 – 249, https://doi.org/10.1016/j.epsl.2016.09.021, 2017.

Jeltsch-Thömmes, A. and Joos, F.: Carbon Cycle Responses to Changes in Weathering and the Long-Term Fate of Stable Carbon Isotopes, Paleoceanography and Paleoclimatology, 38, e2022PA004 577, https://doi.org/https://doi.org/10.1029/2022PA004577, 2023.

Köhler, P.: Atmospheric CO_2 concentration based on boron isotopes versus simulations of the global carbon cycle during the Plio-Pleistocene, Paleoceanography and Paleoclimatology, 38, e2022PA004 439, https://doi.org/10.1029/2022PA004439, 2023.

Köhler, P. and Bintanja, R.: The carbon cycle during the Mid Pleistocene Transition: the Southern Ocean Decoupling Hypothesis, Climate of the Past, 4, 311–332, https://doi.org/10.5194/cp-4-311-2008, 2008.

Köhler, P. and Mulitza, S.: No detectable influence of the carbonate ion effect on changes in stable carbon isotope ratios (δ^{13}C) of shallow dwelling planktic foraminifera over the past 160 kyr, Climate of the Past, 20, 991–1015, https://doi.org/10.5194/cp-20-991-2024, 2024.

Köhler, P. and Munhoven, G.: Late Pleistocene carbon cycle revisited by considering solid Earth processes, Paleoceanography and Paleoclimatology, 35, e2020PA004 020, https://doi.org/10.1029/2020PA004020, 2020.

Köhler, P. and van de Wal, R. S. W.: Interglacials of the Quaternary defined by northern hemispheric land ice distribution outside of Greenland, Nature Communications, 11, 5124, https://doi.org/10.1038/s41467-020-18897-5, 2020.

Köhler, P., Fischer, H., and Schmitt, J.: Atmospheric $\delta^{13}CO_2$ and its relation to pCO_2 and deep ocean δ^{13}C during the late Pleistocene, Paleoceanography, 25, PA1213, https://doi.org/10.1029/2008PA001703, 2010.

Köhler, P., Skinner, L. C., and Adolphi, F.: Radiocarbon cycle revisited by considering the bipolar seesaw and benthic ^{14}C data, Earth and Planetary Science Letters, 640, 118 801, https://doi.org/10.1016/j.epsl.2024.118801, 2024.

Krauss, F.: Insights into the past global carbon cycle and fluctuations of the stable carbon isotopic composition, PhD thesis, University of Bern, Bern, Switzerland, 2024.

Kutterolf, S., Jegen, M., Mitrovica, J. X., Kwasnitschka, T., Freundt, A., and Huybers, P. J.: A detection of Milankovitch frequencies in
global volcanic activity, Geology, 41, 227–230, https://doi.org/10.1130/G33419.1, 2013.

Kutterolf, S., Schindlbeck, J., Jegen, M., Freundt, A., and Straub, S.: Milankovitch frequencies in tephra records at volcanic arcs:
The relation of kyr-scale cyclic variations in volcanism to global climate changes, Quaternary Science Reviews, 204, 1 – 16,
https://doi.org/10.1016/j.quascirev.2018.11.004, 2019.

Laskar, J., Robutel, P., Joutel, F., Gastineau, M., Correia, A. C. M., and Levrard, B.: A long term numerical solution for the insolation
quantities of the Earth, Astronomy and Astrophysics, 428, 261–285, https://doi.org/10.1051/0004-6361:20041335, 2004.

Lisiecki, L. E.: Atlantic overturning responses to obliquity and precession over the last 3 Myr, Paleoceanography, 29, 71–86,
https://doi.org/10.1002/2013PA002505, 2014.

Lisiecki, L. E. and Raymo, M. E.: A Pliocene-Pleistocene stack of 57 globally distributed benthic δ^{18}O records, Paleoceanography, 20,
PA1003, https://doi.org/10.1029/2004PA001071, 2005.

Ma, W., Tian, J., Li, Q., and Wang, P.: Simulation of long eccentricity (400-kyr) cycle in ocean carbon reservoir during
Miocene Climate Optimum: Weathering and nutrient response to orbital change, Geophysical Research Letters, 38, L10701,
https://doi.org/10.1029/2011GL047680, 2011.

Menking, J. A., Shackleton, S. A., Bauska, T. K., Buffen, A. M., Brook, E. J., Barker, S., Severinghaus, J. P., Dyonisius, M. N., and Petrenko,
V. V.: Multiple carbon cycle mechanisms associated with the glaciation of Marine Isotope Stage 4, Nature Communications, 13, 5443,
https://doi.org/10.1038/s41467-022-33166-3, 2022.

Mix, A. C., Le, J., and Shackleton, N. J.: Benthic foraminiferal stable isotope stratigraphy of Site 846: 0-1.8 Ma, in: Proceedings of the
Ocean Drilling Program, Scientific Results Vol 138, edited by Pisias, N. G., Mayer, L., Janecek, T., Palmer-Julson, A., and van Andel, T.,
pp. 839–854, College Station, Texas, USA, https://doi.org/10.2973/odp.proc.sr.138.160.1995, 1995a.

Mix, A. C., Pisias, N. G., Rugh, W., Wilson, J., Morey, A., and Hagelberg, T. K.: Benthic foraminiferal stable isotope record from
site 849 (0-5 Ma): local and global climate changes, in: Proceedings of the Ocean Drilling Program, Scientific Results Vol 138,
edited by Pisias, N. G., Mayer, L., Janecek, T., Palmer-Julson, A., and van Andel, T., pp. 371–412, College Station, Texas, USA,
https://doi.org/10.2973/odp.proc.sr.138.120.1995, 1995b.

Paillard, D.: The Plio-Pleistocene climatic evolution as a consequence of orbital forcing on the carbon cycle, Climate of the Past, 13, 1259–
1267, https://doi.org/10.5194/cp-13-1259-2017, 2017.

Pälike, H., Norris, R. D., Herrle, J. O., Wilson, P. A., Coxall, H. K., Lear, C. H., Shackleton, N. J., k. Tripati, A., and Wade, B. S.: The
heartbeat of the Oligocene climate system, Science, 314, 1894–1898, doi: 10.1126/science.1133822, 2006.

Pisias, N. G. and Moore-Jr., T. C.: The evolution of Pleistocene climate: a time series approach, Earth and Planetary Science Letters, 52,
450–458, https://doi.org/10.1016/0012-821X(81)90197-7, 1981.

Poore, H. R., Samworth, R., White, N. J., Jones, S. M., and McCave, I. N.: Neogene overflow of Northern Component Water at the Greenland-
Scotland Ridge, Geochem. Geophys. Geosyst., 7, Q06010, https://doi.org/10.1029/2005GC001085, 2006.

Prokoph, A., Shields, G., and Veizer, J.: Compilation and time-series analysis of a marine carbonate δ^{18}O, δ^{13}C, ^{87}Sr/^{86}Sr and δ^{34}S database
through Earth history, Earth-Science Reviews, 87, 113 – 133, https://doi.org/10.1016/j.earscirev.2007.12.003, 2008.

R Core Team: R: A Language and Environment for Statistical Computing, R Foundation for Statistical Computing, Vienna, Austria, https:
//www.R-project.org, 2023.

470 Rial, J., Pielke, R. A., Beniston, M., Claussen, M., Canadell, J., Cox, P., Held, H., de Noblet-Ducoudré, N., Prinn, R., Reynolds, J. F., and Salas, J.: Nonlinearities, Feedbacks and Critical Thresholds within the Earth's Climate System, Climatic Change, 65, 11–38, https://doi.org/10.1023/B:CLIM.0000037493.89489.3f, 2004.

Rial, J. A.: Pacemaking the Ice Ages by frequency modulation of Earth's orbital eccentricity, Science, 285, 564–568, https://doi.org/10.1126/science.285.5427.564, 1999.

475 Roesch, A. and Schmidbauer, H.: WaveletComp: Computational Wavelet Analysis, https://CRAN.R-project.org/package=WaveletComp, r package version 1.1, 2018.

Russon, T., Paillard, D., and Elliot, M.: Potential origins of 400-500 kyr periodicities in the ocean carbon cycle: A box model approach, Global Biogeochemical Cycles, 24, GB2013, https://doi.org/10.1029/2009GB003586, 2010.

Sano, Y. and Williams, S. N.: Fluxes of mantle and subducted carbon along convergent plate boundaries, Geophysical Research Letters, 23, 480   2749–2752, https://doi.org/10.1029/96GL02260, 1996.

Schmittner, A., Gruber, N., Mix, A. C., Key, R. M., Tagliabue, A., and Westberry, T. K.: Biology and air-sea gas exchange controls on the distribution of carbon isotope ratios (δ^{13}C) in the ocean, Biogeosciences, 10, 5793–5816, https://doi.org/10.5194/bg-10-5793-2013, 2013.

Schneider, R., Schmitt, J., Köhler, P., Joos, F., and Fischer, H.: A reconstruction of atmospheric carbon dioxide and its stable carbon isotopic composition from the penultimate glacial maximum to the last glacial inception, Climate of the Past, 9, 2507–2523, 485   https://doi.org/10.5194/cp-9-2507-2013, 2013.

Shackleton, N. J. and Opdyke, N. D.: Oxygen-isotope amd paleomagnetic stratigraphy of Pacific core V28-239: Late Pliocene to latest Pleistocene, in: Investigation of Late Quaternary Paleoceanography, and Paleoclimatology, edited by Cune, R. M. and Hays, J. D., vol. 145 of *Geological Society of America Memoir*, pp. 449–464, https://doi.org/10.1130/MEM145-p449, 1976.

Shackleton, N. J., Hall, M. A., and Pate, D.: Pliocene stable isotope stratigraphy of site 846, in: Proceedings of the Ocean Drilling Program, 490   Scientific Results Vol 138, edited by Pisias, N. G., Mayer, L., Janecek, T., Palmer-Julson, A., and van Andel, T., pp. 337–355, College Station, Texas, USA, https://doi.org/10.2973/odp.proc.sr.138.1171995, 1995.

Spero, H. J., Bijma, J., Lea, D. W., and Bemis, B. E.: Effect of seawater carbonate concentration on foraminiferal carbon and oxygen isotopes, Nature, 390, 497–500, https://doi.org/10.1038/37333, 1997.

The MathWorks Inc.: MATLAB Version: 9.14.0.2206163 (R2023a), Natick, Massachusetts, United States, https://www.mathworks.com, 495   2023.

Wang, P., Tian, J., and Lourens, L. J.: Obscuring of long eccentricity cyclicity in Pleistocene oceanic carbon isotope records, Earth and Planetary Science Letters, 290, 319 – 330, https://doi.org/10.1016/j.epsl.2009.12.028, 2010.

Wang, P., Li, Q., Tian, J., Jian, Z., Liu, C., Li, L., and Ma, W.: Long-term cycles in the carbon reservoir of the Quaternary ocean: a perspective from the South China Sea, National Science Review, 1, 119–143, https://doi.org/10.1093/nsr/nwt028, 2014.

500 Westerhold, T., Marwan, N., Drury, A. J., Liebrand, D., Agnini, C., Anagnostou, E., Barnet, J. S. K., Bohaty, S. M., De Vleeschouwer, D., Florindo, F., Frederichs, T., Hodell, D. A., Holbourn, A. E., Kroon, D., Lauretano, V., Littler, K., Lourens, L. J., Lyle, M., Pälike, H., Röhl, U., Tian, J., Wilkens, R. H., Wilson, P. A., and Zachos, J. C.: An astronomically dated record of Earth's climate and its predictability over the last 66 million years, Science, 369, 1383–1387, https://doi.org/10.1126/science.aba6853, 2020.

Whitmeyer, S. J. and Karlstrom, K. E.: Tectonic model for the Proterozoic growth of North America, Geosphere, 3, 220–259, 505   https://doi.org/10.1130/GES00055.1, 2007.

Willeit, M., Ganopolski, A., Calov, R., and Brovkin, V.: Mid-Pleistocene transition in glacial cycles explained by declining CO_2 and regolith removal, Science Advances, 5, eaav7337, https://doi.org/10.1126/sciadv.aav7337, 2019.

Yun, K.-S., Timmermann, A., Lee, S.-S., Willeit, M., Ganopolski, A., and Jadhav, J.: A transient coupled general circulation model (CGCM) simulation of the past 3 million years, Climate of the Past, 19, 1951–1974, https://doi.org/10.5194/cp-19-1951-2023, 2023.

510 Zeebe, R. E., Westerhold, T., Littler, K., and Zachos, J. C.: Orbital forcing of the Paleocene and Eocene carbon cycle, Paleoceanography, 32, 440–465, https://doi.org/10.1002/2016PA003054, 2017.

Zhang, R., Li, X., Xu, Y., Li, J., Sun, L., Yue, L., Pan, F., Xian, F., Wei, X., and Cao, Y.: The 173-kyr Obliquity Cycle Pacing the Asian Monsoon in the Eastern Chinese Loess Plateau From Late Miocene to Pliocene, Geophysical Research Letters, 49, e2021GL097 008, https://doi.org/10.1029/2021GL097008, 2022.